Author/s:
Xu, M;Vidler, C;Wang, J;Chen, X;Pan, Z;Harley, WS;Lee, PVS;Collins, DJ

Title:
Micro-Acoustic Holograms for Detachable Microfluidic Devices

Date:
2024-06-05

Citation:
Xu, M., Vidler, C., Wang, J., Chen, X., Pan, Z., Harley, W. S., Lee, P. V. S. & Collins, D. J. (2024). Micro-Acoustic Holograms for Detachable Microfluidic Devices. Small, 20 (23), https://doi.org/10.1002/smll.202307529.

Persistent Link:
https://hdl.handle.net/11343/340254

RESEARCH ARTICLE

NANO · MICRO small
www.small-journal.com

Micro-Acoustic Holograms for Detachable Microfluidic Devices

*Mingxin Xu, Callum Vidler, Jizhen Wang, Xi Chen, Zijian Pan, William S. Harley, Peter V. S. Lee, and David J. Collins**

Acoustic microfluidic devices have advantages for diagnostic applications, therapeutic solutions, and fundamental research due to their contactless operation, simple design, and biocompatibility. However, most acoustofluidic approaches are limited to forming simple and fixed acoustic patterns, or have limited resolution. In this study,a detachable microfluidic device is demonstrated employing miniature acoustic holograms to create reconfigurable, flexible, and high-resolution acoustic fields in microfluidic channels, where the introduction of a solid coupling layer makes these holograms easy to fabricate and integrate. The application of this method to generate flexible acoustic fields, including shapes, characters, and arbitrarily rotated patterns, within microfluidic channels, is demonstrated.

1. Introduction

Microfluidics has emerged as an important toolkit for medicine,[1,2] chemistry,[3–5] nanotechnology,[6,7] and biomedical science.[8–12] Microfluidic devices offer unique advantages over conventional laboratory techniques due to their compact nature, low fabrication cost, rapid turnaround time, and precise microenvironment control.[13–18] Several approaches have been developed to actively achieve micromanipulation in microfluidic devices, including microgrippers,[19,20] electrowetting,[21–23] and magnetic[24–26] optical[27,28] and acoustic[29–33] forces. Among these methods, acoustic methods have been widely used due to their advantages in being contactless, biocompatible, and ability to achieve manipulation on cellular length scales.[34–36]

In acoustic microfluidic devices such acoustic fields typically form pressure field patterns comprising nodal/antinodal positions, and are used to translate and pattern droplets, particles, and cells.[37,38] These acoustic fields can be generated as lines,[39–42] grids,[43,44] and diffractive patterns conformal to channel interfaces.[32,45–47] The acoustic approaches that result in these patterns, however, have limited ability to generate more complex acoustic fields or reconfigurability. While more complex patterns can be generated by trapping microparticles using microstructures in microfluid channel via acoustic-structure interactions,[48–50] these methods require the fabrication and introduction of additional structures within the channel itself, and can only be used to create fixed acoustic patterns. The use of robot-assisted acoustic flow control, however, has been demonstrated to be multifunctional in pumping, micro-particle capture, liquid mixing, and droplet merging, achieved by generating microflows at the end of capillaries in a way that is modifiable in space using a multi-axis orientation system,[51] albeit outside of the context of microfluidic devices. While progress continues to be made, it has been identified that the development of high-resolution, complex, and configurable patterns in microfluidic platforms has important implications for biomedical applications.[52,53]

More recently, the principles of acoustic holography have demonstrated the ability to create genuinely arbitrary acoustic configurations, with the ability to control the aggregation of wavefronts at a target plane via phase- or amplitude-based holograms.[54–56] Accordingly, acoustic holograms with centimeter-scale apertures have demonstrated the ability to precisely generate complex acoustic fields,[55,57–59] though their application to microscale devices has to date been limited. Efforts have recently sought to miniaturize acoustic holograms, through a mechanism by which particle aggregation often utilizes an air-water interface, rather than using closed microfluidic channels.[60–62] Further, while reconfigurable/switchable acoustic holograms benefit from the implementation of binary amplitude holograms, where optical or electronic signals can be used to generate or control acoustic energies, these contain much less information than phase holograms and thus the reconstructed image resolution is limited.[61,62] Moreover, previous acoustic holograms implementations utilize water coupling layers, which presents difficulties in setup and handling, and further permits the generating or trapping of wavefront-distorting bubbles at the

M. Xu, C. Vidler, J. Wang, X. Chen, Z. Pan, W. S. Harley, P. V. S. Lee, D. J. Collins
Department of Biomedical Engineering
University of Melbourne
Melbourne, Victoria 3010, Australia
E-mail: david.collins@unimelb.edu.au
P. V. S. Lee, D. J. Collins
Graeme Clarke Institute
University of Melbourne
Parkville, Victoria 3052, Australia

The ORCID identification number(s) for the author(s) of this article can be found under https://doi.org/10.1002/smll.202307529

DOI: 10.1002/smll.202307529

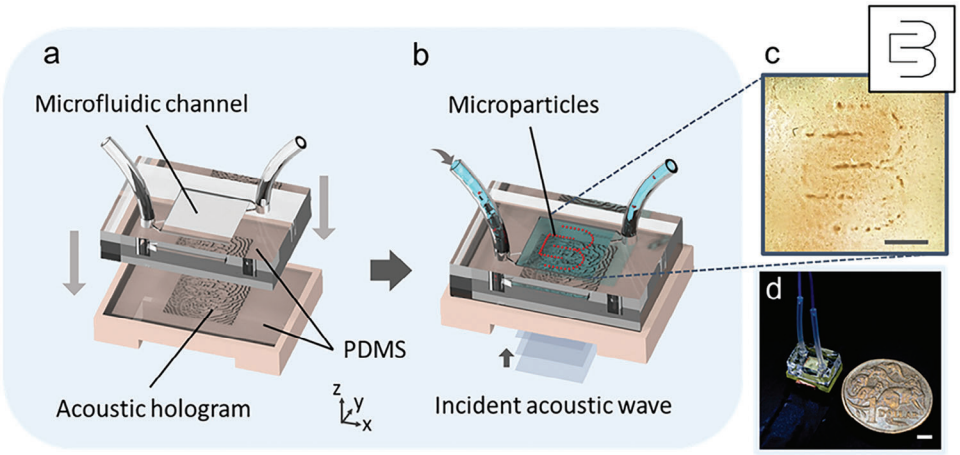

Figure 1. Schematic diagram of acoustic holography for detachable microfluidic devices. a) Detachable microfluidic channels coupled with acoustic holograms via a PDMS coupling layer. b) The incident acoustic waves are modulated by the hologram and then pass through the coupling layer and generate targeted acoustic patterns in the microfluidic channels, which are visualized by the microparticles. c) Experimental result for the logo of Collins Biomicrosystems Lab, where inset shows the input image. d) Fabricated detachable holographic microfluidic device. Scale bars are 1 mm.

hologram surface because of cavitation[63] or decrease in gas solubility with temperature change.[64]

In this work, we demonstrate the smallest reported phase-modulating acoustic hologram that we use to generate designed acoustic fields in closed microchannels. Here the acoustic waves modulated by the micro-hologram enter the microfluidic channel through a Polydimethylsiloxane (PDMS) coupling layer to generate acoustic patterns with high resolution. The micro-holograms are printed by a projection micro stereolithography (PμSL) system[65] and the PDMS coupling layer provides ease of integration. The use of solid PDMS coupling layer, rather than a liquid one, radically simplifies system handling and readily permits the coupling, detachment, and rotation of micro-holograms to generate reconfigurable acoustic patterns a fluid channel. This work overcomes obstacles commonly faced in microfluidic devices, enabling arbitrary and active particle manipulation. Moreover, whereas previous acoustic hologram approaches utilized open containers, here we demonstrate the formation of acoustic patterns in the closed channels more common to microfluidic devices. This approach can accordingly generate flexible, reconfigurable, high-resolution acoustic fields in miniaturized microfluidic systems, where its straightforward fabrication and integration make this broadly appropriate for micromanipulation for biomedical applications.

2. Results and Discussion

The creation of complex acoustic patterns has included the use of binary acoustic holograms due to their simplicity and ease of fabrication using traditional lithography processes,[60–62] though the information embedded within a binary acoustic amplitude-based hologram approach is limited. In contrast, the required resolution and scale of phase holograms at the microscale precludes the use of typical additive manufacturing methods, where the typical ≈0.1–1 mm scale printing resolution used elsewhere limits the hologram resolution and range of acoustic frequencies that can be applied.[55,66] To address this latter point, here we utilize a previously reported projection micro-stereolithography system[65] (detailed in Experimental Section) to print phase micro-holograms.

Detachable microfluidic acoustic holography is a combination of detachable microfluidic channels and acoustic holograms, where a microfluidic channel fabricated from polydimethylsiloxane (PDMS) is coupled to a 3D-printed hologram by the PDMS coupling layer (**Figure 1a**). The incident acoustic wave propagates into the hologram from the transducer along $+z$ and is modulated. After propagating through the PDMS layers, the target acoustic field is generated in a microfluidic channel (Figure 1b), where the resulting acoustic field is visualized via colored PDMS microparticles (Figure 1c, showing the logo of Collins Biomicrosystems Lab). The fabricated holographic microfluidic device with a 5 mm × 5 mm microfluidic domain (holographic aperture), and an overall size of 13.5 mm × 9.5 mm × 2 mm, is smaller than an Australian one-dollar coin (Figure 1d). The microfluidic channels can be easily disassembled, and reused, and can be placed at an angle to the hologram. Therefore, the acoustic field in the microfluidic channel can be switched between different patterns, or where the pattern can be positioned/rotated in the channel via appropriate placement. The detailed dimensions are shown in Figure S3 (Supporting Information).

PDMS has an acoustic impedance comparable to that of water. Therefore, the acoustic wavefront propagating in the PDMS coupling layer can be effectively introduced into the water-filled microfluidic channel with a PDMS coupling layer between the hologram and the microfluidic channel.[67,68] In addition, the solid PDMS coupling layer facilitates device integration without the potential for generating air bubbles in the water coupling layer, and where the microchannel height constrains the fluid domain rather than necessitating the calibration of the required volume of fluid in an open vessel, as in previous acoustic holography implementations.

Figure 2a illustrates the device structure and wave propagation. When incident acoustic waves of 6.9 MHz pass into the 3D-printed hologram that encodes phase information, the acoustic

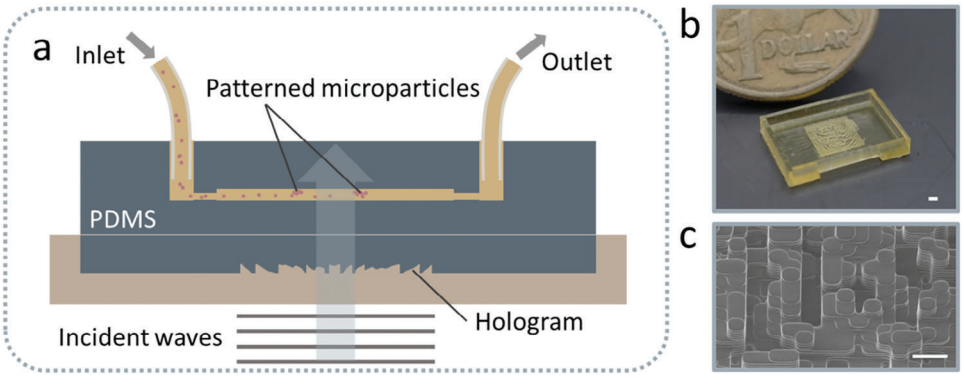

Figure 2. Principle of the detachable holographic microfluidic devices. a) The incident acoustic waves modulated by the hologram pass through the PDMS coupling layer and generate acoustic patterns in the microfluidic channels, where microparticles are patterned by acoustic forces. b) The 3D-printed micro-hologram without PDMS coupling layer, where the aperture of the hologram is 5 × 5 mm. Scale bar is 1 mm. c) Helium ion microscope image for micro-hologram. Scale bar is 100 µm.

waves are modulated. The modulated acoustic waves then pass through the PDMS coupling layer and enter the microchannel to generate a designed acoustic field, whereby particles suspended in the solution are patterned by the acoustic forces. A surfactant solution mixed with polydisperse PDMS particles (<30 µm in diameter) is injected into the microfluidic channel through the inlet. See Experimental Section for design and fabrication details.

Figure 2b shows a hologram with 125 × 125 pixels printed by a custom projection micro-stereolithography system (detailed in Experimental Section), where each pixel has a lateral dimension of 40 µm. The maximum pixel size of a hologram is determined by sampling theorem, which limits the pixel size to less than half the wavelength to avoid aliasing effects. Therefore, the maximum lateral dimension of pixel is limited to ≈107 µm for the 6.9 MHz frequency used in this work. Further, increases in the phase shift ($\Delta\varphi$) are generated by increasing the height of each pixel (H_p, and $\Delta\varphi \propto H_p$), resulting in a maximum pixel height of ≈280 µm for a 2π phase shift at 6.9 MHz, where the speed of sound of the printed hologram is ≈2400 m s^{-1}. It is worth noting that the z-axis printing accuracy is related to the continuity of the phase change, with thinner layer heights resulting in improved, and where the printed layer thickness here is ≈15 µm. Figure 2c shows a representative helium ion microscope image for a printed micro-hologram.

The design and results of detachable microfluidic holography are shown in **Figure 3**. Initially, the target image (Figure 3a, logo of Collins Biomicrosystems Lab (CBML)) is used as the input image, whereafter the phase map of the desired hologram (Figure 3b) is calculated by the iterative angular spectrum method (IASA, see Experimental Section for details). Next, the phase map and accompanying PDMS mold are transformed into an STL file and printed using the projection micro-stereolithography (PμSL) system. The PDMS is then mixed, degassed, and poured into the hologram mold (Figure 3c). The PDMS layer is cured at room temperature (Figure 3d) and acts as the coupling layer between the hologram and the microfluidic channel (Figure 3e). After inflowing the fluid containing PDMS microparticles, the target acoustic field is visualized with the application of an acoustic field from a 500 µm thick $LiNbO_3$ transducer actuated at 6.9 MHz (Figure 3f). The experimental results (Figure 3g) show that the desired acoustic field (Figure 3 h) is generated. The mean squared error (MSE) and structural similarity (SSIM, calculated using MATLAB 2022a, MathWorks, CA, USA) between the normalized grayscale simulation result and experimental result are 0.026 and 0.47, respectively. The distance between the hologram and the microfluidic channel is 2 mm, in which the thickness of the PDMS coupling layer and the PDMS substrate of the microfluidic channel are both 1 mm. The height of the fluid domain in the microfluidic channel is 130 µm. Figures S1 and S2 (Supporting Information) show the resolution of the acoustic field and the schematic diagram of particle transfer in the channel, respectively.

We further investigated the performance of microfluidic acoustic holography for generating various patterns. The "UoM" letters (**Figure 4a**) representing the initials for the University of Melbourne, clearly demonstrate the ability for this method to generate flexible acoustic patterns in microfluidic channels. Experimental results show that the micro-acoustic holograms achieve highly controllable phase modulation, enabling these designed patterns to be clearly displayed within the microfluidic channel.

The angles of microfluidic channels and acoustic holograms can be flexibly reconfigured, as shown in Figure 4b–d. These results demonstrate that different acoustic field orientations can be generated by adjusting the angle of the microfluidic channel, where the target acoustic field is designed as a series of parallel fringes with a spacing of 500 µm. Whereas the spacing between fringes is typically a function of the acoustic wavelength in other acoustofluidic devices,[40,69] here the use of an acoustic hologram permits arbitrary spacing between patterning lines. The angle of the acoustic fringes generated in the microfluidic channel can also be readily adjusted by changing the angle between the microfluidic channel and the hologram part. Notably, the use of a hologram approach in a microchannel rather than one that necessitates the introduction of acoustic energies parallel to the channel plane (i.e., surface acoustic waves) negates the impact of undesired acoustic diffraction, which otherwise results in acoustic fields that are parallel with channel walls.[70,71]

To determine the effect of design parameters on hologram performance while retaining the design of an acoustic hologram

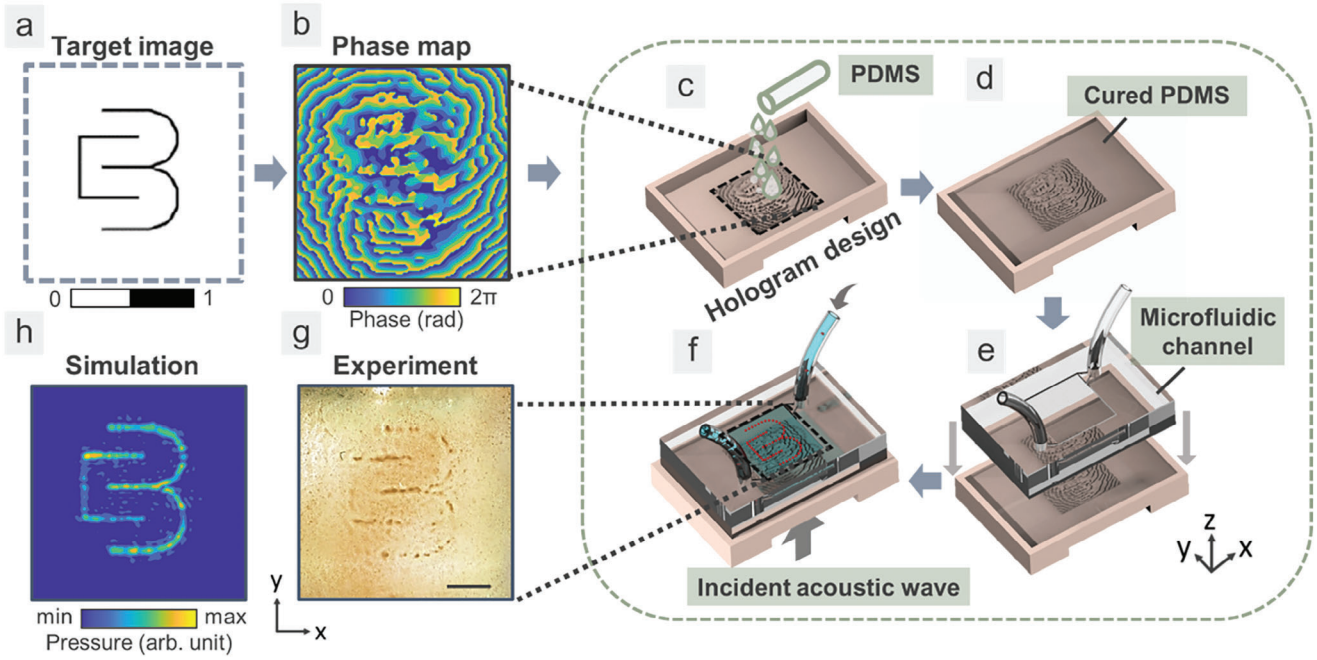

Figure 3. Design and results of detachable holographic microfluidic device. See Experimental Section for details regarding the design and manufacturing. a) A binary image of the lab logo is input as a target image and computed as b) a phase map. c) The hologram model including phase information is 3D printed and filled with PDMS. d) After the PDMS is cured, e) the microfluidic channel is placed on top. f) Injecting microparticles into the microfluidic channel, where the incident acoustic wave is modulated by the hologram and passes through the PDMS coupling layer to pattern the microparticles. g) The experimental image shows that the microparticle pattern obtained corresponds to h) the simulation result.

image at a target plane in the microchannel, **Figure 5** shows the effect of PDMS coupling layer thickness (H_{PDMS}) and fluid domain thickness (H_{fluid}) on image quality. The image quality is represented by peak signal-to-noise ratio (PSNR), where an increased PSNR indicates better image quality (better consistency with the input image). The numbers 0–9, letters A–J, and lab logo are used as the input images, the corresponding input images are shown in Figure S5 (Supporting Information).

Figure 5a demonstrates the degradation of image quality as H_{PDMS} increases from ≈2 mm. The diffraction of acoustic waves in an acoustic hologram is critical for producing shape acoustic patterns.[55] When the acoustic wave propagates to a region

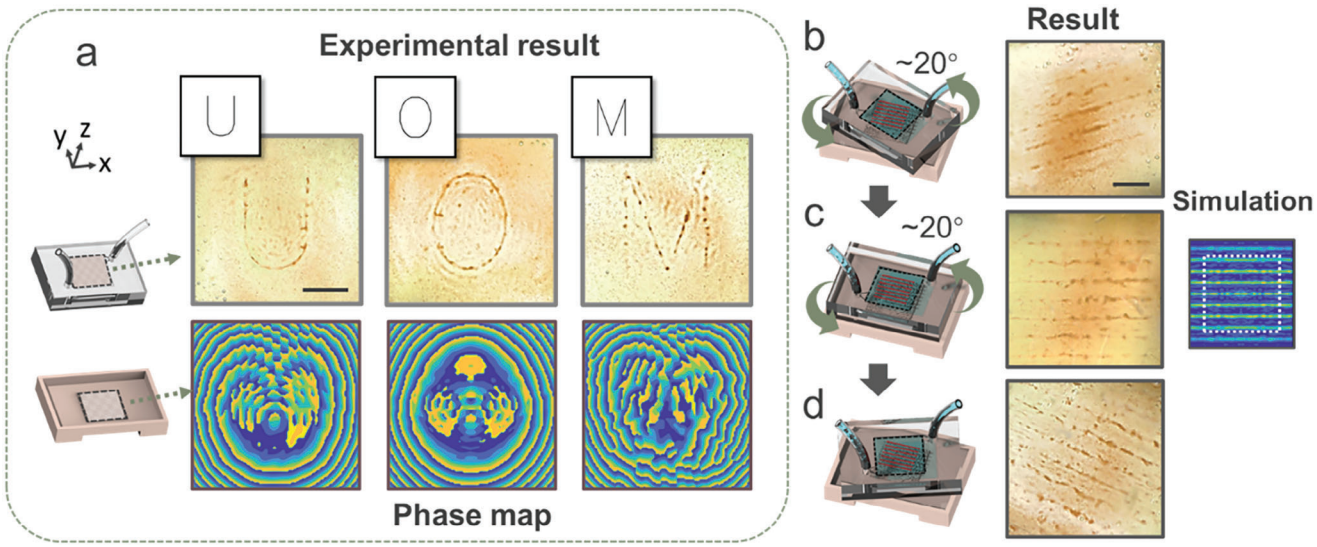

Figure 4. Holographic pattern generation in microfluidic devices, for a) letters "UoM" (standing for the University of Melbourne). b–d) Rotating acoustic fringes, where the microfluidic channels and holograms can be angled to generate acoustic fields with different configurations while using the same hologram. The measured line spacings of the experimental results are shown in Figure S4 (Supporting Information). Scale bars are 1 mm.

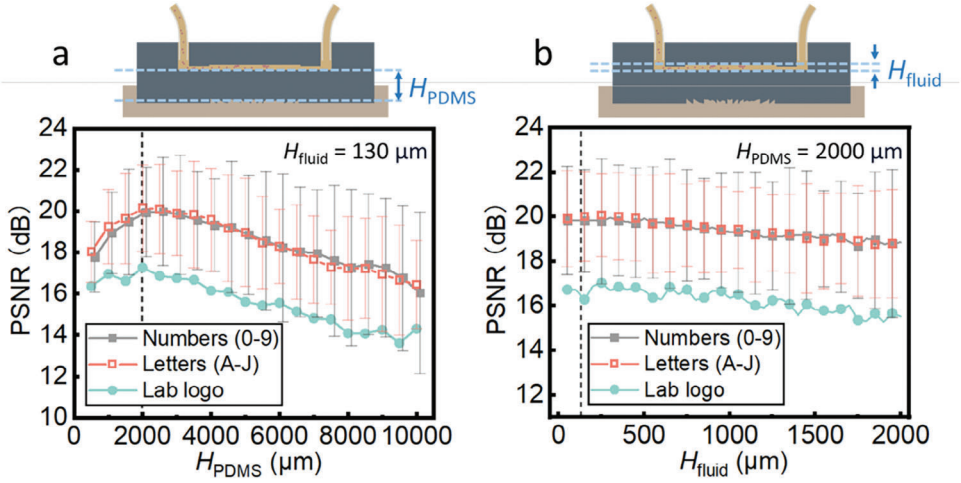

Figure 5. Effect of coupling layer thickness (H_{PDMS}) and fluid domain thickness (H_{fluid}) on image quality. a) Relationship between H_{PDMS} and PSNR for H_{fluid} = 130 μm, where PSNR indicates the image quality. b) Results of changing H_{fluid}, where H_{PDMS} = 2000 μm.

far away from the hologram with far-field conditions, the wavefronts of the Fraunhofer diffraction gradually are gradually flattened, where a flattened wavefront indicates that the phase of the incident waves has limited variation in space, resulting in a degraded diffraction pattern. On the contrary, when the hologram is close to the target plane (H_{PDMS} <2 mm), the effective diffraction angle of the acoustic wave is reduced. In this region the limited wavefront interference degrades the quality of the reconstructed image. Finally, increased target image complexity reduces the resulting image quality as well, with the more complex lab logo resulting in a lower PSNR than the more straightforward letters and numbers.

The relationship between fluid domain height and image quality in microfluidic channels is further shown in Figure 5b, where fluid domain height (H_{fluid}) varies from 50 to 2000 μm and H_{PDMS} = 2000 μm. The results show that the image quality is not significantly affected by the height of the fluid domain within common μm-mm ranges of fluid domain height.[72–74]

In recent years, precise patterning of particles or cells within hydrogels has become of interest in fields including biomedical engineering, tissue engineering, cell engineering, and 3D printing.[75] The patterning different types of particles or cells within a hydrogel matrix has emerged as a promising tool. However, current approaches are still limited by complex fabrication or operations, or limited pattern complexity. In this work, an acoustic holography-based microchannel-based approach provides a new tool for micromanipulation in microfluidic systems. Here, control over the fluid environment is enabled by the use of a microfluidic channel, where the use of optical patterning and acoustic holography can be used to create defined patterns, including heterogeneous microscale patterns in a hydrogel.

Figure 6 shows the patterning of different particles in photocurable hydrogels. A hydrogel (poly(ethylene glycol) diacrylate (PEDGA), see Experimental Section for preparation) with blue particles is injected into the microfluidic channel (Figure 6a) and patterned by acoustic waves (Figure 6b). The patterned blue particles are locally fixed as the photocurable hydrogel is exposed to ultraviolet (UV) light in a selected region (Figure 6c). The uncured hydrogel is subsequently flushed with hydrogel containing green particles (Figure 6d), where the green particles are recolored red for ease of visualization by image processing software (identical image processing on all areas of the image; Photoshop 2022, Adobe, CA, USA) which are then patterned (Figure 6e) and fixed with UV exposure (Figure 6f), resulting in different particles are patterned and fixed in the hydrogel. Figure 6h–j shows the experimental results corresponding to Figure 6b,d,g.

3. Conclusion

Acoustic holography has the unique ability to generate designed acoustic fields, with prior demonstrations evidencing the ability to pattern particles and cells for engineered tissues and materials. Whereas previous implementations of acoustic holography, however, have been generally implemented in open-air chambers and containers, with dimensions of the resulting acoustic target field being on the order of centimeters, here we demonstrate the generation of acoustic holograms for microchannel-based actuation. This permits the ability to realize advantages in terms of liquid handling and control that closed channels afford. Further, the use of immersed transducers in prior setups complicates the switching between different acoustic holograms. To realize this, we fabricate detachable holographic microfluidic devices using a micro-acoustic hologram, comprising a 5 × 5 mm aperture and resulting mm-scale hologram images. Acoustic waves coupled from the transducer are modulated by the 3D-printed hologram, enabling the generation of high-resolution acoustic patterns in a microfluidic channel, where these channels can be coupled/detached/rotated with micro-holograms to generate reconfigurable acoustic patterns. Compared to the prior use of liquid-coupled acoustic holograms, the use of a solid PDMS coupling layer instead facilitates ready integration with microfluidic channels, where the defined height of these layers simplifies alignment and use. We demonstrate this method in the generation of lines, shapes, and characters in microchannels, evidencing the ability to create acoustic holograms within and on the scale of microfluidic devices.

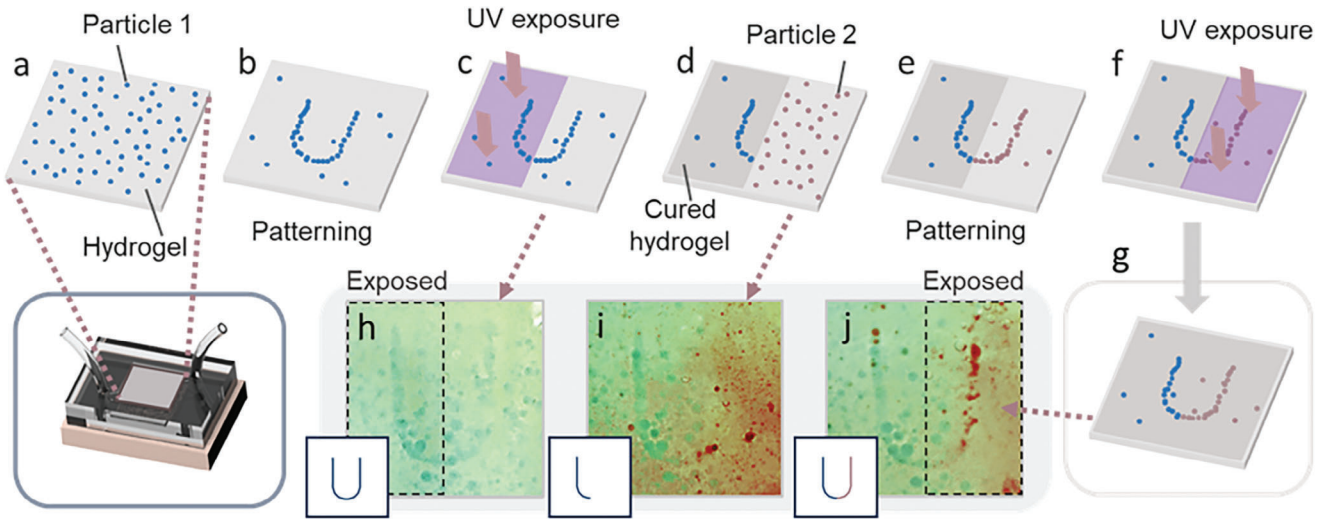

Figure 6. Patterning different types of particles within a hydrogel. a) Hydrogel (see Experimental Section for preparation) containing blue particles is injected into the microfluidic channel and b) patterned with the holographic acoustic field. c) Hydrogel is cured locally by UV exposure. d) Hydrogel containing green particles is injected into the uncured area. The green particles are then e) patterned and f) exposed. g) Cured hydrogels with different types of particles. h–j) Experimental results corresponding to (c,d,g), respectively. Experiments are conducted using blue and green PDMS particles, where the green particles are digitally recolored red to improve visualization.

4. Experimental Section

Design of Acoustic Hologram: The iterative angular spectroscopy method (IASA)[76] was used to calculate the acoustic hologram phase distribution. The calculation procedures were as follows.

1) The complex pressure field of the holographic plane was transformed into an angular spectrum through Fourier transform.
2) The angular spectrum was propagated along +*z* to the image plane by multiplying with the transfer function.
3) The angular spectrum in the image plane was transformed into a complex pressure field via an inverse Fourier transform.
4) The amplitude of the image plane was reset to the input value.
5) The Fourier transform was applied to convert the reset complex pressure field in the image plane into an angular spectrum. 6. The angular spectrum of image plane along -*z* was back-propagated to the hologram plane.
6) The angular spectrum in the hologram plane was transformed into a complex pressure field via an inverse Fourier transform, and reset the amplitude of the complex pressure field to this field.

The above steps were then repeated until a satisfactory target image is obtained, where an iteration number of 150 was used in this work. After 150 iterations, the phase in the complex pressure field of the hologram plane was converted to a 3D model by

$$T_p = \frac{\Delta\varphi}{(k_{PDMS} - k_h)} + T_0 \quad (1)$$

where T_p is the thickness of the pixel, $\Delta\varphi$ is the phase shift. $T_0 =$ 8 mm is the substrate thickness and $\Delta\varphi$ is set to zero at T_0. The parameters k_{PDMS} and k_h are the wavenumbers in PDMS and the hologram material, respectively. The thickness map, including the thickness of each pixel (T_p), was exported as an STL file using a MATLAB code. This model was then combined with the pre-drawn PDMS container in Chitubox software (CBD-Tech, Guangdong, China) and exported as a new STL file.

Fabrication of Micro Holograms: The pillar resolution and scale of the micro-holograms precluded the use of conventional additive manufacturing methodologies, as they fall short of providing the necessary resolution. To facilitate the creation of such holograms, a custom projection micro-stereolithography (PμSL) system[65,77–79] was utilized, capable of achieving an optical resolution of 1 micron and a total printing area of 100 mm x 100 mm. In the PμSL system, UV light was emitted by a high-resolution projector and focused onto the liquid photocurable resin. Under exposure to UV light, the resin cured and formed a thin layer of the desired hologram. The platform was then moved on the *z*-axis to create the desired pattern in the different layers. Each hologram design is initially segmented into layers using Chitubox software (CBD-Tech, Guangdong, China), with each layer measuring 15 μm in height, and subsequently printed onto a photocurable acrylate-based material (HTL Resin, Boston Microfabrication, MA, USA). Each STL file including thickness map and PDMS mold was initially segmented into layers using Chitubox software (CBD-Tech, Guangdong, China), with each layer measuring 15 μm in height, and subsequently printed using a photocurable acrylate-based material (HTL Resin, Boston Microfabrication, MA, USA) using a high-resolution printing system.[65] The dimensions of hologram aperture were 5 × 5 mm and the whole hologram part was ≈13.5 × 9.5 × 2 mm, with a fabrication time of 1.5 h per design. After printing, the holograms were sonicated in isopropyl alcohol for 10 min to remove any excess material and gently dried under a stream of nitrogen. Once dried, the holograms were placed into an 80 °C oven for 24 h to evaporate any surface solvents that would prevent the PDMS from adequately curing in the mold. The PDMS (SYLGARD 184, Dow, MI, USA) with 10:1 mix ratio was then poured into the printed part and left on a level surface for at least 48 h to cure. The thickness of PDMS coupling layer was 2 mm.

Fabrication of Microfluid Channels: SU-8 3050 was spin-coated on silicon wafers at 500 rpm for 10 s followed by 1250 rpm at 30 s, and baked, exposed, and developed according to the manufacturer's manual, where the size of each microfluidic channel was 5 × 5 mm and the thickness was ≈130 μm (see Figure S6, Supporting Information, for the fabrication results). A 10:1 mix of PDMS (SYLGARD 184, Dow, MI, USA) was then poured onto the fabricated mold and cured for 48 h at room temperature on a level surface. The bottom substrate of the microfluidic channel with a thickness of 1 mm was fabricated using PDMS cured on a blank silicon substrate. The bottom substrates and upper microfluidic channels were surface treated by a plasma cleaner (PE-50, Plasma Etch, NV, USA) for 15 s with oxygen and then bonded.

Fabrication of Colored PDMS Microparticles: A 10:1 mix of PDMS (SYLGARD 184, Dow, MI, USA) was added to ≈2 wt.% of a silicone pigment (Orange Silicone Pigment, Barnes, NSW, Australia) and stirred well, then

added to the solution with 1 wt.% Pluronic F-127 (Sigma–Aldrich, MO, USA). The mixture was homogenized for a total of 20 min at room temperature, followed by stirring for 4 h at 40 °C and leaving at room temperature for at least 1 day to cure.

Preparation of Photocurable Hydrogel: The hydrogel monomer, poly(ethylene glycol) diacrylate (PEGDA, M_n = 700 g mol^{-1}, Sigma–Aldrich, MO, USA), was fully dissolved in deionized water at a weight ratio of 1:4. The PEGDA solution was then mixed with 0.25 wt.% photoinitiator (Lithium phenyl (2,4,6-trimethylbenzoyl) phosphinate (LAP), Sigma–Aldrich, MO, USA). To cure the hydrogel with the microfluidic channels, a Digital Light Processing (DLP) module (DLPLCR4500EVM, Texas Instruments, TX, USA) was used to expose the local area for 80 s from the top of the channel.

Experiment Setup: The combination of microfluidic channels and micro-holograms was placed on the surface of an acoustic transducer, where a thin layer of ultrasound transmission gel (Aquasonic 100, Parker Laboratories, NJ, USA) was used for coupling between the transducer and hologram. The acoustic transducers were fabricated by depositing Cr/Al films on both sides of a 500 µm thick lithium niobate (128°Y-cut $LiNbO_3$) wafer. The suspension with PDMS microparticles (see the previous section for preparation) was injected into the channel with a syringe connected by polytetrafluoroethylene (PTFE) tubing. A power amplifier (TBMDA4B, Tekbox, Ho Chi Minh City, Vietnam) and a function generator (AFG 31 252, Tektronix, OR, USA) provided a 6.9 MHz sine wave at ≈1 W to drive the transducer. The patterns in the microfluidic channels were recorded by a camera (37MP HDMI USB Camera, Eakins, Guangdong, China) mounted on a stereo microscope (Stemi 508, ZEISS, Jena, Germany).

Supporting Information

Supporting Information is available from the Wiley Online Library or from the author.

Acknowledgements

The authors thank Mr. Philipp Segeritz, Dr. Melanie Stamp, Mr. Michael Halwes, Mr. Bram Servais, and Prof. Zhichao Ma for their appreciated technical assistance. This work was performed in part at the Melbourne Centre for Nanofabrication (MCN) in the Victorian Node of the Australian National Fabrication Facility (ANFF). Dr. Collins is the recipient of a Discovery Early Career Researcher Award and Discovery Project from the Australian Research Council (DECRA, DE200100909; DP, DP230102550), and funding from the National Health and Medical Research Council (Ideas, APP2003446).

Open access publishing facilitated by The University of Melbourne, as part of the Wiley - The University of Melbourne agreement via the Council of Australian University Librarians.

Conflict of Interest

The authors declare no conflict of interest.

Data Availability Statement

The data that support the findings of this study are available in the supplementary material of this article.

Keywords

acoustic hologram, detachable, fluid manipulation, microfluidics, micromanipulation

Received: August 29, 2023
Revised: November 24, 2023
Published online:

[1] Y. Ma, C. Liu, S. Cao, T. Chen, G. Chen, *J. Mater. Chem. B* **2023**, *11*, 546.
[2] M. Kumar Thimmaraju, R. Trivedi, G. Hemalatha, B. Thirupathy, A. Mohathasim Billah, *Mater Today Proc.* **2023**, https://doi.org/10.1016/j.matpr.2023.03.096.
[3] W. Alahmad, P. Varanusupakul, P. Varanusupakul, *Crit. Rev. Anal. Chem.* **2023**, *53*, 233.
[4] P. Roszkowska, A. Dickenson, J. E. Higham, T. L. Easun, J. L. Walsh, A. G. Slater, *Lab Chip* **2023**, *23*, 2720.
[5] A. Goralczyk, F. Mayoussi, M. Sanjaya, S. F. Corredor, S. Bhagwat, Q. Song, S. Schwenteck, A. Warmbold, P. Pezeshkpour, B. E. Rapp, *Chem. Ing. Tech.* **2022**, *94*, 975.
[6] A. Giorello, A. Nicastro, C. L. A. Berli, *Adv. Mater. Technol.* **2022**, *7*, 2101588.
[7] Z. Fattahi, M. Hasanzadeh, *Tren. Analyti. Chem.* **2022**, *152*, 116637.
[8] J. Sateesh, K. Guha, A. Dutta, P. Sengupta, D. Yalamanchili, N. S. Donepudi, M. Surya Manoj, S. S. Sohail, *Biomicrofluidics* **2022**, *16*, 41501.
[9] C. Shao, J. Chi, L. Shang, Q. Fan, F. Ye, *Acta Biomater.* **2022**, *138*, 21.
[10] Z. Wei, S. Wang, J. Hirvonen, H. A. Santos, W. Li, *Adv. Healthcare Mater.* **2022**, *11*, 2200846.
[11] Z. Chen, S. Kheiri, E. W. K. Young, E. Kumacheva, *Langmuir* **2022**, *38*, 6233.
[12] S. Preetam, B. K. Nahak, S. Patra, D. C. Toncu, S. Park, M. Syväjärvi, G. Orive, A. Tiwari, *Biosens. Bioelectron. X* **2022**, *10*, 100106.
[13] S. Battat, D. A. Weitz, G. M. Whitesides, *Lab Chip* **2022**, *22*, 530.
[14] K. Raj M, S. Chakraborty, *J. Appl. Polym. Sci.* **2020**, *137*, 48958.
[15] H. Fallahi, J. Zhang, H.-P. Phan, N.-T. Nguyen, *Micromachines* **2019**, *10*, 830.
[16] A. V. Nielsen, M. J. Beauchamp, G. P. Nordin, A. T. Woolley, *Annu. Rev. Anal. Chem.* **2020**, *13*, 45.
[17] V. Ortseifen, M. Viefhues, L. Wobbe, A. Grünberger, *Front. Bioeng. Biotechnol.* **2020**, *8*, 589074.
[18] J. B. Nielsen, R. L. Hanson, H. M. Almughamsi, C. Pang, T. R. Fish, A. T. Woolley, *Anal. Chem.* **2020**, *92*, 150.
[19] Z.-C. Ma, J. Fan, H. Wang, W. Chen, G.-Z. Yang, B. Han, *Small* **2023**, *19*, 2300469.
[20] J.-C. Kuo, H.-W. Huang, S.-W. Tung, Y.-J. Yang, *Sens. Actuators A Phys.* **2014**, *211*, 121.
[21] R. B. Fair, V. Srinivasan, H. Ren, P. Paik, V. K. Pamula, M. G. Pollack, in *IEEE Int. Electron Devices Meeting*, IEEE, Piscataway, NJ **2003**.
[22] M. G. Pollack, V. K. Pamula, V. Srinivasan, A. E. Eckhardt, *Expert Rev. Mol. Diagn.* **2011**, *11*, 393.
[23] M. G. Pollack, A. D. Shenderov, R. B. Fair, *Lab Chip* **2002**, *2*, 96.
[24] D. Lombardi, P. S. Dittrich, *Anal. Bioanal. Chem.* **2011**, *399*, 347.
[25] M. A. M. Gijs, F. Lacharme, U. Lehmann, *Chem. Rev.* **2010**, *110*, 1518.
[26] Y. Zhang, N.-T. Nguyen, *Lab Chip* **2017**, *17*, 994.
[27] L. C. Geonzon, M. Kobayashi, T. Sugimoto, Y. Adachi, *Colloids Surf A Physicochem Eng. Asp.* **2022**, *642*, 128691.
[28] K. T. Kotz, K. A. Noble, G. W. Faris, *Appl. Phys. Lett.* **2004**, *85*, 2658.
[29] D. J. Collins, Z. Ma, J. Han, Y. Ai, *Lab Chip* **2017**, *17*, 91.
[30] H. Afsaneh, R. Mohammadi, *Talanta Open* **2022**, *5*, 100092.
[31] D. J. Collins, B. Morahan, J. Garcia-Bustos, C. Doerig, M. Plebanski, A. Neild, *Nat. Commun.* **2015**, *6*, 8686.
[32] M. Xu, P. V. S. Lee, D. J. Collins, *Lab Chip* **2022**, *22*, 90.
[33] Y. Li, S. Cai, H. Shen, Y. Chen, Z. Ge, W. Yang, *Biomicrofluidics* **2022**, *16*, 31502.
[34] J. Friend, L. Y. Yeo, *Rev. Mod. Phys.* **2011**, *83*, 647.
[35] P. Zhang, H. Bachman, A. Ozcelik, T. J. Huang, *Annu. Rev. Anal. Chem.* **2020**, *13*, 17.
[36] A. Ozcelik, J. Rich, T. J. Huang, *Multidisciplinary Microfluidic and Nanofluidic Lab-on-a-chip*, Elsevier, Amsterdam Netherlands **2022**.
[37] Y. Gao, M. Wu, Y. Lin, J. Xu, *Micromachines* **2020**, *11*, 921.

[38] L. Y. Yeo, J. R. Friend, *Annu. Rev. Fluid Mech.* **2014**, *46*, 379.
[39] Y. Chen, A. A. Nawaz, Y. Zhao, P.-H. Huang, J. P. Mccoy, S. J. Levine, L. Wang, T. J. Huang, *Lab Chip* **2014**, *14*, 916.
[40] J. Shi, X. Mao, D. Ahmed, A. Colletti, T. J. Huang, *Lab Chip* **2008**, *8*, 221.
[41] Z. Mao, Y. Xie, F. Guo, L. Ren, P.-H. Huang, Y. Chen, J. Rufo, F. Costanzo, T. J. Huang, *Lab Chip* **2016**, *16*, 515.
[42] D. J. Collins, C. Devendran, Z. Ma, J. W. Ng, A. Neild, Y. Ai, *Sci. Adv.* **2016**, *2*, e1600089.
[43] G. Destgeer, H. J. Sung, *Lab Chip* **2015**, *15*, 2722.
[44] Y. Wang, Y. Wang, D. Mei, Z. Yu, D. Xue, *Biodes. Manuf.* **2020**, *3*, 87.
[45] D. J. Collins, R. O'rorke, C. Devendran, Z. Ma, J. Han, A. Neild, Y. Ai, *Phys. Rev. Lett.* **2018**, *120*, 74502.
[46] Y. Bian, F. Guo, S. Yang, Z. Mao, H. Bachman, S.-Y. Tang, L. Ren, B. Zhang, J. Gong, X. Guo, T. J. Huang, *Microflu. Nanoflu.* **2017**, *21*, 132.
[47] K. Kolesnik, P. Hashemzadeh, D. Peng, M. E. M. Stamp, W. Tong, V. Rajagopal, M. Miansari, D. J. Collins, *Phys. Rev. E* **2021**, *104*, 45104.
[48] K. Kolesnik, P. Segeritz, D. J. Scott, V. Rajagopal, D. J. Collins, *Lab Chip* **2023**, *23*, 2447.
[49] W. S. Harley, K. Kolesnik, M. Xu, D. E. Heath, D. J. Collins, *Adv. Funct. Mater.* **2022**, *33*, 2211422.
[50] X. Bai, S. Bin, D. Yuguo, Z. Wei, F. Yanmin, C. Yuanyuan, Z. Deyuan, A. Fumihito, F. Lin, *Sens. Actuators A Phys.* **2020**, *315*, 112340.
[51] J. Durrer, P. Agrawal, A. Ozgul, S. C. F. Neuhauss, N. Nama, D. Ahmed, *Nat. Commun.* **2022**, *13*, 6370.
[52] D. B. Go, M. Z. Atashbar, Z. Ramshani, H.-C. Chang, *Anal. Methods* **2017**, *9*, 4112.
[53] A. Lenshof, M. Evander, T. Laurell, J. Nilsson, *Lab Chip* **2012**, *12*, 684.
[54] J. D. Maynard, E. G. Williams, Y. Lee, *J. Acoust. Soc. Am.* **1985**, *78*, 1395.
[55] K. Melde, A. G. Mark, T. Qiu, P. Fischer, *Nature* **2016**, *537*, 518.
[56] M. Xu, W. S. Harley, Z. Ma, P. V. S. Lee, D. J. Collins, *Adv. Mater.* **2023**, *35*, 2208002.
[57] Z. Ma, A. W. Holle, K. Melde, T. Qiu, K. Poeppel, V. M. Kadiri, P. Fischer, *Adv. Mater.* **2020**, *32*, 1904181.
[58] M. D. Brown, B. T. Cox, B. E. Treeby, *Appl. Phys. Lett.* **2020**, *116*, 261901.
[59] M. D. Brown, *Appl. Phys. Lett.* **2019**, *115*, 53701.
[60] M. D. Brown, J. Jaros, B. T. Cox, B. E. Treeby, *J. Acoust. Soc. Am.* **2016**, *139*, 1637.
[61] Y. Gu, C. Chen, J. Rufo, C. Shen, Z. Wang, P.-H. Huang, H. Fu, P. Zhang, S. A. Cummer, Z. Tian, T. J. Huang, *ACS Nano* **2020**, *14*, 14635.
[62] Z. Ma, K. Melde, A. G. Athanassiadis, M. Schau, H. Richter, T. Qiu, P. Fischer, *Nat. Commun.* **2020**, *11*, 4537.
[63] T. Lyubimova, K. Rybkin, O. Fattalov, M. Kuchinskiy, L. Filippov, *Ultrasonics* **2021**, *117*, 106516.
[64] R. Battino, T. R. Rettich, T. Tominaga, *J. Phys. Chem. Ref. Data* **1984**, *13*, 563.
[65] C. Vidler, K. Crozier, D. Collins, *Microsyst. Nanoeng.* **2023**, *9*, 67.
[66] M. Xu, J. Wang, W. S. Harley, P. V. S. Lee, D. J. Collins, *Adv. Sci.* **2023**, *10*, 2301489.
[67] Z. Ma, D. J. Collins, Y. Ai, *Anal. Chem.* **2016**, *88*, 5316.
[68] I. Leibacher, S. Schatzer, J. Dual, *Lab Chip* **2014**, *14*, 463.
[69] X. Ding, S.-C. S. Lin, M. I. Lapsley, S. Li, X. Guo, C. Y. Chan, I.-K. Chiang, L. Wang, J. P. Mccoy, T. J. Huang, *Lab Chip* **2012**, *12*, 4228.
[70] C. Devendran, K. Choi, J. Han, Y. Ai, A. Neild, D. J. Collins, *Lab Chip* **2020**, *20*, 2674.
[71] D. J. Collins, R. O'rorke, A. Neild, J. Han, Y. Ai, *Soft Matter* **2019**, *15*, 8691.
[72] O. Vanderpoorten, Q. Peter, P. K. Challa, U. F. Keyser, J. Baumberg, C. F. Kaminski, T. P. J. Knowles, *Microsyst. Nanoeng.* **2019**, *5*, 40.
[73] O. Kaspar, A. H. Koyuncu, A. Hubatová-Vacková, M. Balouch, V. Tokárová, *RSC Adv.* **2020**, *10*, 15179.
[74] A. Grimes, D. N. Breslauer, M. Long, J. Pegan, L. P. Lee, M. Khine, *Lab Chip* **2008**, *8*, 170.
[75] W. S. Harley, C. C. Li, J. Toombs, C. D. O'connell, H. K. Taylor, D. E. Heath, D. J. Collins, *Bioprinting* **2021**, *23*, e00147.
[76] S. Mellin, G. Nordin, *Opt. Express* **2001**, *8*, 705.
[77] Q. Ge, Z. Li, Z. Wang, K. Kowsari, W. Zhang, X. He, J. Zhou, N. X. Fang, *Int. J. Extreme Manuf.* **2020**, *2*, 022004.
[78] C. Sun, N. Fang, D. M. Wu, X. Zhang, *Sens. Actuators A Phys.* **2005**, *121*, 113.
[79] D. Han, C. Yang, N. X. Fang, H. Lee, *Addit. Manuf.* **2019**, *27*, 606.